Langmuir
Article
pubs.acs.org/Langmuir

Tailoring Anisotropic Wetting Properties on Submicrometer-Scale Periodic Grooved Surfaces

Deying Xia,[†,⊥] Xiang He,[†] Ying-Bing Jiang,[‡] Gabriel P. Lopez,[§] and S. R. J. Brueck*[,†]

[†]*Center for High Technology Materials and Department of Electrical and Computer Engineering, University of New Mexico, 1313 Goddard, SE, Albuquerque, New Mexico 87106,* [‡]*Center for Micro-Engineered Materials, University of New Mexico, Albuquerque, New Mexico 87131, and* [§]*Center for Biomedical Engineering and Department of Chemical and Nuclear Engineering, University of New Mexico, Albuquerque, New Mexico 87131.* [⊥]*Current Address: Department of Materials Science and Engineering, Massachusetts Institute of Technology, 77 Massachusetts Avenue, Cambridge, MA 02139, USA.*

Received July 24, 2009. Revised Manuscript Received December 29, 2009

The use of simple plasma treatments and polymer deposition to tailor the anisotropic wetting properties of one-dimensional (1D) submicrometer-scale grooved surfaces, fabricated using interferometric lithography in photoresist polymer films, is reported. Strongly anisotropic wetting phenomena are observed for as-prepared 1D grooved surfaces for both positive and negative photoresists. Low-pressure plasma treatments with different gas compositions (e.g., CHF_3, CF_4, O_2) are employed to tailor the anisotropic wetting properties from strongly anisotropic and hydrophobic to hydrophobic with very high contact angle and superhydrophilic with a smaller degree of wetting anisotropy and without changing the structural anisotropy. The change of the surface wetting properties for these 1D patterned surfaces is attributed to a change in surface chemical composition, monitored using XPS. In addition, the initial anisotropic wetting properties on 1D patterned samples could be modified by coating plasma treated samples with a thin layer of polymer. We also demonstrated that the wetting properties of 1D grooved surfaces in a Si substrate could be tuned with similar plasma treatments. The ability to tailor anisotropic wetting on 1D patterned surfaces will find many applications in microfluidic devices, lab-on-a-chip systems, microreactors, and self-cleaning surfaces.

Introduction

Much progress has been made recently in the preparation of superhydrophobic surfaces, in methods to control the surface wetting properties, and in the fabrication of nanostructured materials responsive to external stimuli for switching wetting properties.[1,2] The methods for controlling surface wetting include different external factors such as temperature,[3] electric field,[4] and chemical modification.[5] Interest in anisotropic wetting phenomena on patterned surfaces has increased as a result of the development of fabrication techniques for well-defined chemically and topographically micro- and nanopatterned surfaces. Potential applications include self-cleaning, biosensing, lab-on-a-chip systems, intelligent membranes, microfluidics, and microreactor systems. Both dynamic (different sliding angles in different directions) and static (different static contact angles in different directions) anisotropic wetting have been observed. In nature, some surfaces demonstrate dynamic anisotropic wetting, for example, rice leaves,[6] butterfly wings,[7] and the Namib Desert beetle.[8] These surfaces have directional adhesion with superhydrophobic wetting and structural anisotropy on micro- and nanoscales.

Inspired by this natural biological analogy and enabled by advances in nanofabrication, researchers have fabricated one-dimensional (1D) micro- and nanopatterned heterogeneous chemical composition and topographical surfaces exhibiting static anisotropic wetting properties.[9,10] In some cases, these 1D structural surfaces can exhibit both static and dynamic anisotropic wetting.[9] The fabrication approaches for 1D micro- and nanogrooved surface include standard photolithography,[11] nanoimprint lithography,[12] interferometric lithography,[13] strained microwrinkling,[10,14] and embossing.[14,15] Experimentally, most of the 1D grooved surfaces investigated have been on micrometer-scale (several to tens of micrometer periodicity) or have involved shallow curved or sinusoidal grooved surfaces, while theoretically, a rectangular cross-section has been assumed in analyzing the anisotropic wetting behavior.[14,16,17] With interference lithography (IL), 1D deep grooved surfaces with rectangular shapes and submicrometer periodicity are easily fabricated for investigation of anisotropic wetting behavior.[18] In our previous work, we

*To whom correspondence should be addressed. E-mail: brueck@chtm.unm.edu.

(1) Li, X.-M.; Reinhoudt, D.; Crego-Calamla, M. *Chem. Soc. Rev.* **2007**, *36*, 1350.
(2) Xia, F.; Jiang, L. *Adv. Mater.* **2008**, *20*, 2842.
(3) Fu, Q.; Rao, G. V. R.; Basame, S. B.; Keller, D. J.; Artyushkova, K.; Fulghum, J. E.; Lopez, G. P. *J. Am. Chem. Soc.* **2004**, *126*, 8904.
(4) Krupenkin, T. N.; Taylor, J. A.; Wang, E. N.; Kolodner, P.; Hodes, M.; Salamon, T. R. *Langmuir* **2007**, *23*, 9128.
(5) Martines, E.; Seunarine, K.; Morgan, H.; Gadegaard, N.; Wilkinson, C. D.; Riehle, M. O. *Nano Lett.* **2005**, *5*, 2097.
(6) Feng, L.; Li, S.; Li, Y.; Li, H.; Zhang, L.; Zhai, J.; Song, Y.; Liu, B.; Jiang, L.; Zhu, D. *Adv. Mater.* **2002**, *14*, 1857.
(7) Zheng, Y.; Gao, X.; Jiang, L. *Soft Matter* **2007**, *3*, 178.
(8) Zhai, L.; Berg, M. C.; Cebeci, F. C.; Kin, Y.; Midwid, G. M.; Cohen, R. E.; Rubner, M. F. *Nano Lett.* **2006**, *6*, 1213.
(9) Morita, M.; Koga, T.; Otsuka, H.; Takahara, A. *Langmuir* **2005**, *21*, 911.
(10) Chung, J. Y.; Youngblood, J. P.; Stafford, C. M. *Soft Matter* **2007**, *3*, 2608.
(11) Sommers, A. D.; Jacobi, A. M. *J. Micromech. Microeng.* **2006**, *16*, 1571.
(12) Zhang, F.; Low, H. Y. *Langmuir* **2007**, *23*, 7793.
(13) Zhao, Y.; Lu, Q.; Li, M.; Li, X. *Langmuir* **2007**, *23*, 6212.
(14) Kusumaatmaja, H.; Vrancken, R. J; Bastiaasen, C. W. M.; Yeomans, J. M. *Langmuir* **2008**, *24*, 7299.
(15) Yang, J.; Rose, f. R. A.; Gadegarrd, N.; Alexander, M. R. *Langmuir* **2009**, *25*, 2567.
(16) Chen, Y.; He, B.; Lee, J.; Patankar, N. A. *J. Colloid Interface Sci.* **2005**, *281*, 458.
(17) Li, W.; Fang, G.; Li, Y.; Qiao, G. *J. Phys. Chem. B* **2008**, *112*, 7234.
(18) Xia, D.; Gamble, T. C.; Mendoza, E. A.; Koch, S. J.; He, X.; Lopez, G. P.; Brueck, S. R. J. *Nano Lett.* **2008**, *8*, 1610.

reported strongly anisotropic wetting on 1D nanopatterned polymer surfaces fabricated with IL and demonstrated the use of silica nanoparticle deposition to tune the surface wetting anisotropy from hydrophobic to hydrophilic.[19] It remains a challenge to develop simple and controllable approaches to tailoring the anisotropic wetting properties on 1D nanopatterned surfaces.

Plasma treatment with different gases is an effective way to control surface wetting. In general, an oxygen plasma is used to adjust the surface wetting to hydrophilic or superhydrophilic,[20,21] while CF_4 and CHF_3 plasmas are used to tailor surface wetting to ultra- or superhydrophobic.[22,23] The advantages of controlling surface wetting with plasma treatment are: it is fast; adjustable (easy to control with plasma gases and parameters); low-temperature (cold plasma, low-pressure reactor); environmentally friendly (absence of organic solutions and rinsing); and amenable to mass production. Most previous reports have been focused on adjusting the wetting properties for plasma treatments of isotropic wetting surfaces. It is necessary to investigate the new phenomena involved in adjusting the wetting behavior on anisotropic wetting surfaces consisting of anisotropic structures with plasma treatment.

Here, we report static anisotropic wetting behavior with a high degree of wetting anisotropy on 1D submicrometer scale periodic grooved surfaces with different surface materials. We also demonstrate simple approaches to tailoring the anisotropic wetting across different wetting conditions and anisotropies with short plasma treatments. Finally, we discuss the surface chemical modifications resulting from these plasma treatments using surface chemical analysis techniques.

Experimental Section

IL with a 355 nm frequency tripled YAG laser source was used to produce 1D periodic patterns. The samples were precleaned with freshly prepared piranha solution (volume ratio 3:1 of concentrated sulfuric acid and hydrogen peroxide solution). A bottom antireflective coating (BARC iCON7 from Brewer Science) layer was spin deposited at 3000 rpm on the precleaned sample followed by baking at 205 °C for 1 min. The final thickness of BARC was around 70 nm. Both positive-tone photoresist (PR, Shipley SPR505A) and negative-tone PR (NR7-500P, NR7-250P, Futurrex, Inc.) were used. SPR 505A was spin deposited at 4000 rpm and baked at 150 °C for 1 min while NR7-500P and NR7-250P were deposited at 4000 rpm and baked at 90 °C for one minute. The PR final thicknesses were 500 nm (SPR 505A), 500 nm (NR7-500P), and 250 nm (NR7-250P). A thicker positive PR layer (~1 μm) was prepared using two cycles of spin-coating of SPR 505A. Parallel, rectangular profile PR groove patterns atop a continuous BARC polymer layer resulted from the exposure, postexposure bake, and develop steps.

Plasma treatment was performed with a standard reactive ion etching (RIE) process. Oxygen, CHF_3, and CF_4 plasma treatments were carried out at a flow rate of 10 sccm, pressure 10 mTorr, RF power 45 W for 20 s, except when otherwise specified.

Most of the results presented below were on PR/BARC structures. Additional investigations were carried out on homogeneous Si material with nanopatterned grooves fabricated with standard semiconductor processing approaches. After forming 1D PR grooves with negative PR, an oxygen plasma with 1 min etch time was used to etch through the BARC. Then, the mixture of O_2 and CHF_3 (flow rate 10 sccm, pressures: O_2 5 mT and CHF_3 90mT, RF power 100 W) was used to etch the Si for 12 min. Finally, the remaining BARC/PR patterns were removed with piranha solution.

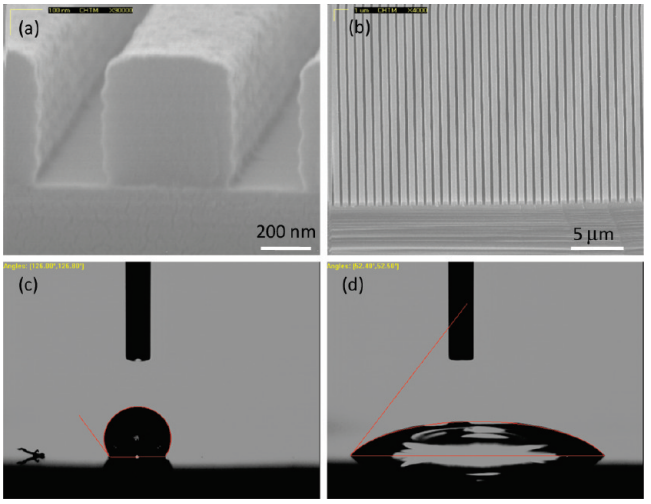

Figure 1. SEM images of 1D negative PR patterns and contact angle images of untreated samples: (a,b) SEM images; (c,d) contact angles θ_x and θ_y.

The change of surface chemical composition with plasma treatment was analyzed with X-ray photoelectron spectroscopy (XPS). XPS measurements were performed on a Kratos Axis Ultra spectrometer using a Al Kα X-ray source. An electron flood gun for charge neutralization and hemispherical analyzer with eight multichannel photomultiplier detector was employed for analysis. The area for the XPS analysis was 700 × 300 μm^2. Three areas on each sample were analyzed for a 90° take-off angle (TOA), 8−10 nm depth. Survey data (low resolution wide scan) was acquired at 80 eV pass energy for 4 min. High resolution spectra were acquired at 20 eV pass energy. All spectra were charge referenced to the aliphatic carbon line at 285.0 eV.

The resulting structures were characterized by field-emission scanning-electron microscopy (FE-SEM, JEOL 6400F) at 30 kV. The static water contact angle (CA) was measured with an AST Products Optima tool. The water drop volume was 2 μL. The data presented for each sample was the average of at least five measurements.

Results and Discussion

With 355 nm IL, we can easily fabricate 1D periodic patterns over a large area with periodicities from 300 to >2000 nm.[24] For a given periodicity, the duty cycle (width of PR wall: width of empty channel) is adjustable with exposure time or power and with the use of different PR materials.

Figure 1 shows SEM images of 1D patterns and corresponding CA measurements using negative PR for an 800 nm pitch groove density (sample A). Well-defined 1D PR patterns with minimal sidewall standing waves were formed atop the BARC layer as shown in Figure 1a. Deep (~500 nm) and narrow (~300 nm) open channels with rectangular cross sections above the BARC layer are evident. Here, the duty ratio is defined as the ratio of width of PR wall to width of open channel while the aspect ratio denotes the ratio of height to the width of the PR wall. The duty ratio is 5:3 for this sample. The uniformity of these 1D patterns is obvious from Figure 1b. The as-prepared 1D nanopatterned surface exhibited strongly anisotropic wetting properties. The CA measured from the direction orthogonal to the PR lines is defined as

(19) Xia, D.; Brueck, S. R. J. *Nano Lett.* **2008**, *8*, 2819.
(20) Minko, S.; Muller, M.; Motornor, M.; Nitshke, M.; Grundke, K.; Stamm, M. *J. Am. Chem. Soc.* **2003**, *125*, 3896.
(21) Dupont-Gillain, Ch.C.; Adriaebsen, Y.; Derclaye, S.; Rouxhet, P. G.; Motornor, M. *Langmuir* **2000**, *16*, 8194.
(22) Hong, Y. C.; Uhm, H. S. *Appl. Phys. Lett.* **2006**, *88*, 24401.
(23) Jokinen, V.; Sainiemi, L.; Franssila, S. *Adv. Mater.* **2008**, *20*, 3453.
(24) Xia, D.; Li, D.; Ku, Z.; Luo, Y.; Brueck, S. R. J. *Langmuir* **2007**, *23*, 5377.

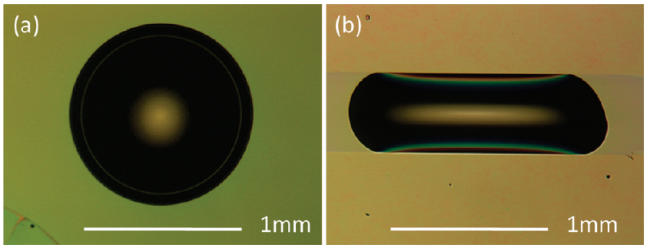

Figure 2. Top view 5× optical microscope images for water droplets on negative PR: (a) 0.25 μL water droplet, unpatterned PR film; (b) 0.15 μL water droplet, 1D PR patterns.

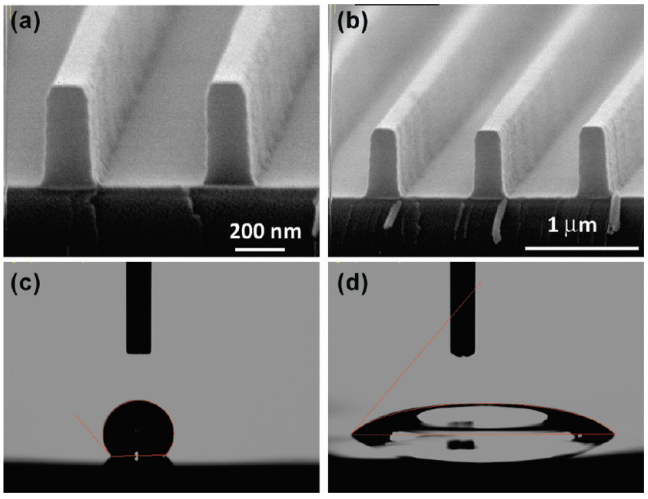

Figure 3. SEM images of 1D positive PR patterns and contact angle images on untreated samples: (a,b) SEM images; (c,d) contact angles θ_x and θ_y.

θ_x and from the direction parallel to the PR lines as θ_y.[19] The wetting anisotropy is $\Delta\theta$ ($= \theta_x - \theta_y$). In addition, the CA measured on an unpatterned PR film is defined as θ_0. For sample A, θ_x was 126° and θ_y was 52° ($\Delta\theta$ = 74°), while θ_0 was only 74°. The wetting was hydrophobic with high contact angle (θ_x = 126°) in the direction perpendicular to the PR lines. It is much more convenient to observe the top-down shape differences of water droplets on these patterned and nonpatterned PR surfaces. From optical microscopy, the water droplet on an unpatterned negative PR film has a symmetric, circular shape, while the water droplet on the 1D patterned negative PR surface exhibits a strongly oblong shape as shown in Figure 2. The deformed shape of the liquid front on the right side of the droplet was caused by an extraneous scratch on the sample.

Similar strongly anisotropic wetting properties were observed on 1D nanopatterned surfaces fabricated with positive PR (sample B) as shown in Figure 3. The 1D PR patterns for a two-cycle spin-coating of SPR 505A are 800 nm high and 250 nm wide, with a periodicity of 1000 nm.

The duty ratio (1:4) of the positive PR, 800 nm pitch pattern in Figure 3 is evidently quite different from that of the negative PR pattern (5:3) in Figure 1. Here, θ_x is 130° and θ_y is 49° ($\Delta\theta$ = 81°), while θ_0 was only 67°. Previously, we have shown that the periodicity of the 1D patterns has only a modest effect on strongly anisotropic wetting.[19] Here, we further conclude that the anisotropy is only weakly dependent on the duty cycle as well. Even though the CA (67°) for this positive PR film (SPR 505A) is lower than that (74°) of the negative PR film (NR7-500P), the observed anisotropy of wetting of the as-prepared 1D structure with positive PR is larger than that on as-prepared 1D structure with negative PR. The somewhat larger wetting anisotropy for this sample mainly results

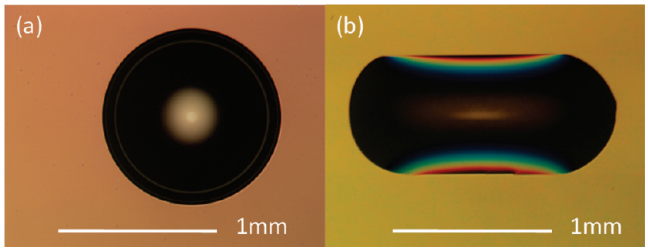

Figure 4. Top view 5× optical microscope images for water droplets on positive PR: (a) 0.25 μL water droplet, unpatterned PR film; (b) 0.15 μL water droplet, 1D PR patterns.

Table 1. Contact Angle Data on 1D Patterned Sample

	original			CHF_3 plasma			O_2 plasma		
sample	θ_0 (°)	θ_x (°)	θ_y (°)	θ_0 (°)	θ_x (°)	θ_y (°)	θ_0 (°)	θ_x (°)	θ_y (°)
(A) negative PR	74	126	52	111	127	108	< 5	0	0
(B) positive PR	67	130	49	100	140	108	0	< 5	0
(C) Si	21	39	33	95	95	79			

from the pattern morphology with the small duty ratio (wide open channels) and high aspect ratio (high PR walls) in sample B. In this case, the morphology of 1D nanostructure plays a more significant role in establishing the anisotropy of the surface wetting than the surface chemistry. The water droplets have a larger energy barrier along the direction perpendicular to the PR lines. Similar phenomena have been observed for 2D surface patterns, a forest of nanopillars exhibits more pronounced water repellency than a comparable nanopit texture.[5] The evident difference of shape of water droplets on 1D patterned and nonpatterned surfaces was observed from optical microscopy as well as shown in Figure 4. It should be noted that the wetting anisotropy on 1D grooved surface is affected by the volume of the measurement droplet.[15]

Both positive and negative 1D PR patterns were treated with CHF_3 and O_2 plasmas to tailor the anisotropic wetting. The highly reproducible results are shown in Table 1. The etching is easy to perform; and the processing parameters in the etch chamber, for example, the etch gases, powers, and times are readily controlled. Different wetting properties in different wetting range and wetting anisotropy could be achieved on the same morphological samples with a short plasma treatment.

First, after a short CHF_3 plasma treatment (20 s), the strongly anisotropic wetting of the original sample is changed to only slightly anisotropic hydrophobic wetting. Visually, the water droplets appeared to be spherical balls on the treated samples (see Supporting Information, Figures S1 and S2) even though our CA data show that the wetting anisotropy, $\Delta\theta$, is 19° for sample A and 32° for sample B. Surface chemical changes are mainly responsible for this change of the surface wetting. The plain PR films without any patterns exhibit isotropic and hydrophobic wetting after CHF_3 plasma treatment (θ_0 is 111° for sample A with negative PR and is 100° for sample B with positive PR). The surface morphology is unchanged by these short plasma treatments. We also investigated the use of CF_4 plasma treatment. Sample A has θ_x 132°, θy 112°, while sample B has θ_x 137°, θ_y 112° after 20 s CF_4 plasma treatment. Therefore, CA data with CF_4 treatment are very similar to the results with CHF_3 treatment. With further CHF_3 plasma treatment, the 1D patterned surfaces exhibit lower anisotropy and become more hydrophobic, even superhydrophobic with possible formation of a hierarchically structured anisotropy.[25] In initial experiments, we observed

(25) Gao, X.; Yao, X.; Jiang, L. *Langmuir* **2007**, *23*, 4886.

an increased surface roughness on the top and side wall surfaces after long durations of CHF_3 plasma treatment. The details of the change of roughness and corresponding change of contact angle with duration of CHF_3 treatment are under investigation.

After a short oxygen plasma treatment (20 s), both sample A and B exhibit ultrahydrophilic wetting with a reduced degree of anisotropy as shown in Table 1. Even though the measurement of CA is almost zero in both directions, stretching of the water droplet along the grating lines is still evident by visual inspection. With longer plasma treatment (60 s), the 1D patterned surfaces exhibit isotropic, superhydrophilic wetting. We can easily tune the anisotropic wetting to hydrophilic wetting by adjusting the parameters in the plasma processing.

The structural changes resulting from the plasma treatments for sample A (negative PR patterns) were investigated with scanning electron microscopy as shown in Figure 5 (also see Supporting Information, Figure S3). After CHF_3 plasma treatment, the PR/BARC patterns are intact with no observable change of dimensions in the 1D structural profile. With the short oxygen plasma treatment, the dimensions of the PR patterns are decreased slightly due to oxygen plasma etching of the polymer. The BARC layer in the spaces between the PR walls is almost entirely etched away as shown in Figure 5d. The similar structural results after short plasma treatment were obtained for sample B (positive PR patterns) as well. Overall, the 1D PR patterns are only slightly modified from the original profiles with the short duration CHF_3 or O_2plasma etching. Therefore, we can tailor anisotropic wetting while retaining the structural anisotropy using simple and controllable plasma treatments.

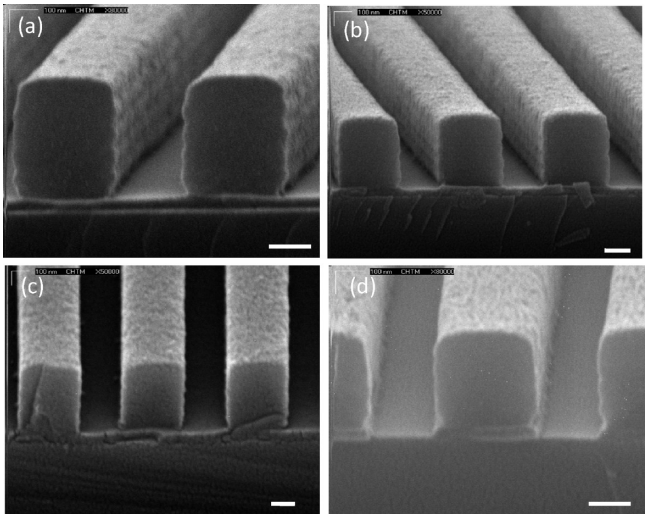

Figure 5. SEM images of 1D negative PR patterns: (a) before CHF_3 plasma treatment; (b) after CHF_3 plasma treatment; (c) before oxygen plasma treatment; (d) after oxygen plasma treatment. Scale bar: 200 nm.

Anisotropic wetting on Si grooves was examined as well. With a simple and straightforward fabrication approach, we can easily fabricate deep and wide 1D Si grooves with longer RIE times (12 min). Here, we used negative PR patterns as the etching mask to produce 1D Si grooves with 500 nm periodicity. Due to the simultaneous etching of the PR as well as the Si with a plasma mixture of CHF_3 and O_2, the resultant deep Si grooves have quite thin Si walls as shown in Figure 6 (sample C). With the more complicated semiconductor processes such as metal deposition and lift-off, we could transfer the IL patterns to Si layer with high fidelity and have well-defined 1D Si structures. The CA data for sample C are shown in Table 1. The original 1D Si grooves, with fresh hydroxyl groups resulting from the final piranha clean, exhibited hydrophilic, slightly anisotropic wetting with $\theta_x = 39°$, $\theta_y = 33°$ and $\Delta\theta = 6°$. A smooth Si surface, after following all the processing steps except the IL exposure, exhibited a CA of $\theta_0 = 21°$. With 20 s of CHF_3 treatment, the wetting moves toward anisotropic wetting ($\theta_x = 95°$, $\theta_y = 79°$ and $\Delta\theta = 16°$). With further CHF_3 treatment (60 s), the surface becomes more hydrophobic and more anisotropic ($\theta_x = 128°$, $\theta_y = 83°$ and $\Delta\theta = 45°$). Anisotropic wetting properties persist in the deep Si grooves as well, and the tailoring approach with plasma treatment is also applicable to 1D Si grooves. The increase of anisotropy on Si patterned surface after CHF_3 treatment is opposite to the trend on PR patterned surfaces after CHF_3 treatment. The differences of wetting anisotropy between Si grooves and PR grooves come from both the chemical composition and the topography of the 1D grooved surfaces.

The surface chemistry of plasma-treated and nontreated samples was investigated by XPS, a sensitive technique to determine the surface composition following the plasma treatment processing. The XPS sampling depth of ~10 nm gives information with regard to the changes in surface chemistry that result from the plasma treatments. The relative atomic concentrations from XPS survey spectra for samples A, B, and C before and after short plasma treatment are listed in Table 2. Changes in the high-resolution C1s and O1s spectra before and after short plasma treatment for sample A are shown in Figure 7.

The two types of PR have different surface compositions from measured atomic concentration due to the different compositions

Table 2. Relative Elemental Compositions (%) Obtained from XPS Analysis

		C	O	F	N	Sb	Si
(A) negative PR	original	79.1	13.8	4.6	2.5		
	20 s CHF_3 plasma	62.9	6.6	29.1	1.4		
	20 s CF_4 plasma	59.8	6.4	32.1	1.7		
	20 s O_2 plasma	66.9	25.1	3.7	2.3	2.0	
	60 s O_2 plasma	60.5	31.5	3.9	1.0	3.1	
(B) positive PR	original	69.8	21.4	1.3	7.5		
	20 s CHF_3 plasma	61.3	10.5	25.3	2.9		
	20 s O_2 plasma	66.4	24.9	2.0	6.1		0.6
(C) Si	original	9.1	40.9				50.0
	20 s CHF_3 plasma	31.5	14.5	23.0			31.0

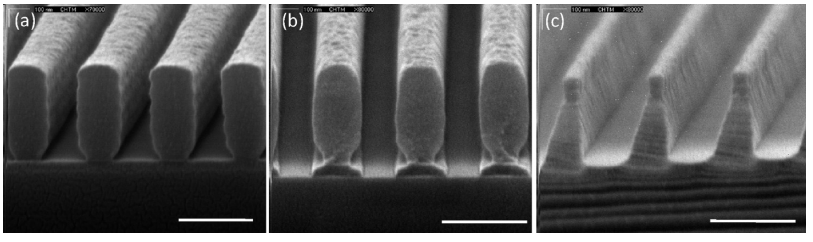

Figure 6. SEM images of deep 1D Si grooves fabricated with negative PR: (a) PR; (b) after etching ARC; (c) Si grooves. Scale bar: 500 nm.

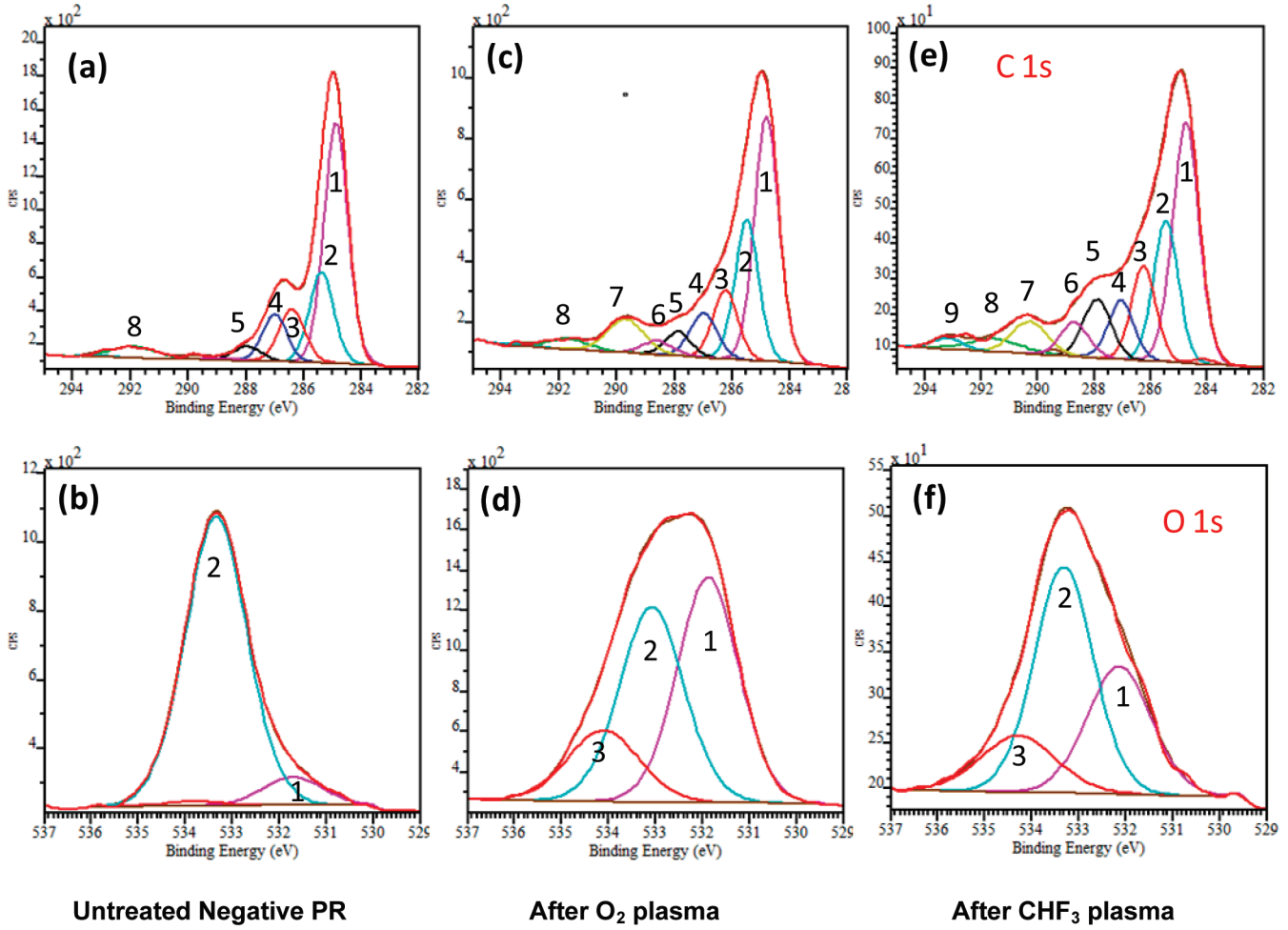

Figure 7. C1s (top row) and O1s (bottom row) XPS spectra with fitted peaks for negative PR: (a,b) untreated PR; (c,d) oxygen plasma treatment; (e,f) CHF_3 plasma treatment. See text for peak assignments.

of the bulk PR solutions and chemical modifications occurring with subsequent exposure and developing process. The different surface compositions for samples A and B results in the slight difference of isotropic wetting properties on the unpatterned PR films. Sample B has more N, C−N, and COOH, while sample A has more of C−C and C*−CO and some C−F species. Particularly, the relatively high fluorine (F) content in sample A (4.6%) compared to sample B (1.3%) contributes the slightly higher CA of sample A (74°) than that of sample B (67°). From Table 2 it is shown that the oxygen (O) content is moderately increased after a short oxygen plasma treatment (20 s), and a further increase is observed for further oxygen plasma treatment (60 s) for PR samples. For example, for sample A, the oxygen (O) content is increased from ~14% to ~25% after a 20 s oxygen plasma treatment and to ~31% after a 60 s oxygen plasma treatment as a result of significant oxidation of the surface. After a short oxygen plasma treatment, the carbon (C) content is decreased slightly because of ashing of the organic component. Other atomic content (F, N) is largely unchanged for a 20 s oxygen plasma treatment. The nitrogen (N) content is decreased from ~2.5% to ~1% for a 60 s oxygen plasma treatment. The ratio of oxygen (O) to carbon (C) determined by XPS is 0.17, 0.38, and 0.52 for untreated, 20 s oxygen treated, and 60 s oxygen treated samples with negative PR, respectively. The ratio of oxygen (O) to carbon (C) is increased from 0.30 to 0.38 after 20 s oxygen plasma treatment for positive PR sample B. There is minimal change of surface roughness and sample morphology during the short oxygen treatment for PR samples A and B, and the cause of change into the hydrophilic wetting range comes mostly from the changes in the surface chemical compositions, such as oxygen and carbon content in the etch process.

After a 20 s CHF_3 plasma treatment, a significant increase of surface fluorine (F) content was observed for all samples. For example, for sample A, the fluorine (F) content is increased from ~5% to ~29% after a 20 s CHF_3 plasma treatment. Similarly, the fluorine (F) content is increased from ~5% to ~32% after a 20 s CF_4 plasma treatment. It is apparent that the low surface energy resulting from the increased fluorine chemical content is responsible for the observed change of surface wetting during a short CHF_3 plasma treatment. As was the case for the O_2 plasma treatment, the roughness of the surface in the short CHF_3 treatment processing is almost unchanged, thus, its contribution to the change of surface wetting is minimal.

We further examined the high resolution spectra for sample A before plasma treatment, after a 20 s oxygen treatment, and after a 20 s CHF_3 plasma treatment. To clarify the precise groups that exist on untreated and treated sample surfaces, a curve fitting analysis of C1s and O1s peaks was performed. The curves in Figure 7 show typical XPS C1s (top) and O1s (bottom) spectra of untreated (left), 20 s oxygen-plasma treated (middle), and 20 s CHF_3-plasma treated (right) samples, respectively. For untreated sample A, the C1s spectrum can be divided into six main peaks at 284.8, 285.5, 286.3, 287.1, 287.9, and 291.6 eV (Figure 7a). These C1s components are assigned, respectively, to the binding energy

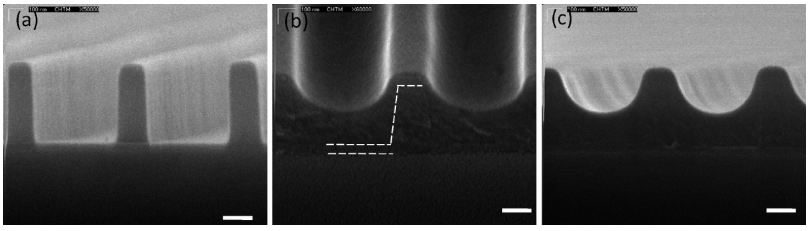

Figure 8. SEM images: (a) 1D positive PR patterns; (b,c) after CHF_3 etching and spin-coating with negative PR. Scale bar: 200 nm.

of C−C (1), C−C=O (2), C−OH (3), C−O−C (4), C=O/N−C=O (5), and CF_2/shakeup (8). The O1s spectrum of untreated sample A is the result of two main components: C=O/C−N=O (1) and C−O (2) (Figure 7b). After a 20 s oxygen plasma treatment, an increase in intensity of peaks due to C=O/N−C=O (5), COOH (6), and NCO_2/C−F (7) was observed in the C1s spectrum due to oxidation of the PR surface (Figure 7c). From the O1s spectrum, after a 20 s oxygen plasma treatment (Figure 7d), additional oxidation of the surface is evident: an increase in O=C (1) and O−C=O (3) is observed. The XPS data suggests that the short oxygen plasma treatment induces mainly formation of C=O and COOH groups.[21,26] The differences in the shape of C1s and O1s after the short oxygen plasma treatment reveal the modifications of the PR surfaces that lead to changes in the surface wetting into the hydrophilic range.

After a short CHF_3 treatment, the evolution of C−F (7) and C−F_3 (9) is clear from the C1s spectrum. In O1s spectrum, the three main peaks come from binding energy for O=C−C−F_x/O−C−F_x (1), C−O (2), and O−C−C−F_x/O−C=O (3) for the CHF_3-treated sample. The feature ascribed to 5 is increased as well after the CHF_3 treatment, possibly due to C−F_x. O−C species decrease from 90% to ∼50% for CHF_3 treatment. Different ratios of acetate-type and ethanol-type binding to C−F_x are observed. The formation of C−F_x during CHF_3 treatment results in the change of the surface wetting from anisotropic to hydrophobic with a smaller degree of anisotropy and a larger contact angle. It is believed that a thin fluorocarbon film is formed during short CHF_3 treatment.[22,23]

The tailoring of surface wetting with a short plasma treatment is mostly caused by the change of surface chemistry during the plasma treatment. However, the surface wetting after plasma treatment is known to age with time and use. A superhydrophilic surface is particularly susceptible to aging. In our preliminary experiments, the superhydrophilic surface is maintained for over two weeks, while the ultrahydrophobic surface can be held for nearly one month. Aging for a more extensive period and strategies to slow aging will be explored in future experiments.

Finally, an additional method to modify the anisotropic wetting of 1D PR patterns was also developed. This is illustrated for positive PR patterns after a short CHF_3 plasma treatment as an example. A thin negative PR (NR7-250P) layer was spun on the CHF_3-treated positive PR patterns samples at a spin speed of 4000 rpm and baked at 90 °C for 1 min. Negative PR was used because the solvents in the positive PR solution would have dissolved the original positive PR pattern. Shallow grooves were formed after spin-coating of the thin polymer, as shown in Figure 8. The interface between the original PR patterns and the covering PR is barely visible in the SEM images and is marked with a white dotted line in Figure 8b. The interface between the BARC and new spin-coating PR is observed also as marked in Figure 8b. Even though the periodicity is retained, the grooves have much shallower and smoother profiles than before. The measured CA data after spin-coating with thin polymer layer are: $\theta_x = 115°$; $\theta_y = 80°$. The wetting anisotropy is not as large as for the original untreated PR pattern as a result of the reduced angularity and depth of the recoated patterns. Through different spin-coating processes (e.g., varying the spin-speed), different resultant profiles of the final polymer (e.g., thickness of negative PR) and, thus, different anisotropic wetting behaviors can be achieved. The morphology of 1D polymer patterns is a very important factor that affects the anisotropic wetting of the 1D structure. Another possible approach to modifying strongly anisotropic wetting is the formation of a conformal layer of polymer by plasma polymer deposition.[27] Cycling between hydrophobic and hydrophilic plasma treatments results in a relatively rapid degradation of the anisotropy over several cycles, probably also as a result of a degraded morphology.

With a combination of IL and conventional lithography, it is straightforward to fabricate integrated micro/nanofluidic devices and lab-on-a-chip systems for many practical applications. Furthermore, using this approach to tune the surface anisotropic wetting properties, we believe that both simple patterned droplets[28,29] and more complex droplets[23] can be formed on predesigned surfaces. Compared to the modification of surface wetting with silica nanoparticles,[19,30] the current short plasma treatment approach results in a much smaller change in the original 1D topography while tuning the surface wetting. Even though the anisotropic wetting behavior exists on morphologically flat and chemically 1D patterned surfaces as well,[31] our as-prepared 1D topographically corrugated surface with tunable anisotropic wetting using plasma treatment offers a convenient means to control fluids in open-channel microfluidic systems.[32] The guided flow of water droplets is another technical application enabled by tailoring anisotropic surfaces.[33,34] The ability to create nanostructured surfaces with different wetting contrasts and wetting anisotropies opens up many exciting applications in biomedicine and biotechnology.[35]

In summary, we report simple and controllable approaches to tailoring strong structurally anisotropic wetting across different wetting ranges (from ultrahydrophobic to ultrahydrophilic) using short plasma treatments. The anisotropic wetting could be

(26) Tsougeni, K.; Vourdas, N.; Tserepi, A.; Gogolides, E. *Langmuir* **2009**, *25*, 11748.
(27) Hirotsu, T.; Castillo, M.; Nakayama, K.; Tsuruta, S.; Suzuki, H. *Thin Solid Films* **2007**, *515*, 4125.
(28) Zhang, X.; Jin, M.; Liu, Z.; Tryk, D. A.; Nishimoto, S.; Murakami, T.; Fujishima, A. *J. Phys. Chem. C* **2007**, *111*, 14521.
(29) Lim, H. S.; Han, J. G.; Kwak, D.; Jin, M.; Cho, K. *J. Am. Chem. Soc.* **2006**, *128*, 14458.
(30) McConnel, M. D.; Bassani, A. W.; Yang, S.; Composto, R. J. *Langmuir* **2009**, *25*, 11014.
(31) Bliznyuk, O.; Vereshchagina, E.; Kooiji, E. S.; Poelsema, B. *Phys. Rev. E* **2009**, *79*, 041601.
(32) Khare, K.; Zhou, J.; Yang, S. *Langmuir* **2009**, *25*, 12794.
(33) Yoshimitsu, Z.; Nakajima, A.; Watanabe, T.; Hashimoto, K. *Langmuir* **2002**, *18*, 5818.
(34) Xu, Q. F.; Wang, J. N.; Smith, I. H.; Sanderson, K. D. *Appl. Phys. Lett.* **2008**, *93*, 233112.
(35) Song, W.; Veiga, D. D.; Custodio, C. A.; Mano, J. F. *Adv. Mater.* **2009**, *21*, 1.

modified with deposition of a thin polymer layer as well. The tuning approach is also applicable to Si grooved surfaces. The surface chemical modification contributes mostly the tuning behavior of surface wetting with a short plasma treatment. These phenomena can be exploited in applications such as microfluidic devices, lab-on-a-chip subsystems, and microreactors.

Acknowledgment. This work was supported by the National Science Foundation under Grant 0515684 and by the Army Research Office. We are grateful to Dr. Kateryna Artyushkova of the University of New Mexico for XPS analysis.

Supporting Information Available: Additional figures, including top-down views of drops on the plane and patterned surfaces and SEM images of PR patterns before and after etch processing, are presented. This material is available free of charge via the Internet at http://pubs.acs.org.